2020年度　芝浦工業大学大学院

修　　士　　論　　文

題目：**Forced convective heat transfer in cylindrical pipe flows**

専攻	理工学研究科（修士課程） 機械工学専攻
学籍番号	MD18060
氏名	Yoshinori Hattori
指導教員	丹下 学

目 次

Nomenclature

Physics Constants

c	Speed of light in a vacuum inertial system	$299,792,458\,m/s$
h	Plank Constant	$6.62607 \times 10^{-34}\,Js$

Material Properties

T	Temperature	K
C_p	Specific heat capasity	$J \cdot kg^{-1}K^{-1}$
λ	Thermal conductivity	$Wm^{-1}K^{-1}$
μ	Dynamic viscosity	$Pa \cdot s$
ρ	Density	kg/m^3
Pr	Prandtl number	-

Other Symbols

ρ	Friction Index
V	Constant Volume

第1章　Introduction

1.1 Study background

Forced convective heat transfer lies at the heart of many aspect of cooling technology and it is therefore desirable to understand its properties as well as possible. Effective cooling technology is constantly being required to wide variety of industrial engineering aplication. To achieve effective coolant system requires comprefensive research of heat transfer coefficient with a wide variety of flow condition. Although many reserchers have been focusing on experimental and computational research, heat transfer coefficient vary with Reynolds number is still unclear. To this end, many reserchers have been focusing on heat transfer from experimental and computational research aspect. However, heat transfer in transitional and turbulent flow is still very challenging task for both experimental and computational research.

1. Experimental research

2. Computational research
   Direct numerical simuration In technology, flows regime and heat transfer plays an important role in considerting engineering issues. Navie-Stokes equations describe the relation of variable flows.

   (1.1)

   However, deterministic solution of the equations are only valid for small disturbances in the initial and boundary condition. In physically, it is hard to get initial and boundary conditions in infinite accurate. Turbulent has a large amount of fluctuations, i.e. turbulent is completely different kind of laminar flows. Direct Numerical Simuration (DNS) is one of the simulation way to predict flow forms. The object of the simuration is to solve the compelete set of equation of motion without using any model. From Kolmogorov lenght scale, total number of cumputations is derivered following equation (1.2). The DNS require large amount of total number of computations.

   $$\mathcal{N} \times \mathcal{M} = \mathcal{O}(Re^{11/4}) \tag{1.2}$$

   The equauation implies the limitation of the DNS and that is directly connected to computer technology. Normally, engineeres is interested in high Reynolds number such as aircraft or atmospheric boundary layer. However, such high Reynolds number requires huge amount of total number of computations and it's far from reality. Large eddy simulation

One attempt to improve our understanding of entanglement is the study of our ability to perform experimental investigation

These coolant technology is used wide varaety of coolant applications such as electric devices, automotive, and plant factory. Considering heat transfer issues, heat transfer coefficients are one of the most important numbers. The Nusselt number (Nu) is a dimensionless number which represents the ratio of convective (h) and conductive heat transfer (k), as expressed in Equation.

1.2 Previous research

The equauation implies the limitation of the DNS and that is directly connected to computer technology. Normally, engineeres is interested in high Reynolds number such as aircraft or atmospheric boundary layer. However, such high Reynolds number requires huge amount of total number of computations and it's far from reality.

Therefore, it is nessesary to get experimental data for correlations of heat transfer and flow condition and the Reynolds number.

Many studies have pointed out that a heat transfer coefficient varies depending on the type of flow: laminar, transition and turbulent. Gnienlinski[4][7] showed a calculation method about heat transfer coefficients for the laminar, transitional and turbulent flows. Bertsche et al.[1] focused on reliable prediction of the heat transfer coefficient for transitional flows. In their study, they showed experimental the heat transfer coefficients for the Reynolds number, $500 < Re < 23000$, and the Prandtl number, $7 < Pr < 41$.

However, not so many data is available for experimental data of laminar-to-turbulent transitional region. More studies should be conducted to obtain experimental data for high the Prandtl number and transitional flows. In this study, the author focused on forced convective heat transfer in flow of water and glycole in a cylindrical pipe. A 50/50vol% mixture of water and glycole, which is a typical liquid coolant in automotive applications, was used as an operating fluid. The experiment was carried out by considering a board range of Reynolds numbers, spanning from a laminar to fully turbulent flow. Moreover, the measurements of the wall friction coefficients was also performed in this study.

1.2.1 Skin friction coefficients

The skin friction coefficients for laminar flow is descrived following equation.

$$C_{f,lam} = \frac{16}{Re_b} \tag{1.3}$$

Konakov[6] showed the skin friction coefficients for turbulent flow.

$$C_{f,turb} = 0.25(1.8log(Re_b) - 1.64)^{-2} \tag{1.4}$$

1.2.2 The heat transfer coefficients

Gunienski [3] showed correlations for each flow conditions: laminar, transitional and turbulent, respectively. Gunienski [3] showed calculation method for laminar flow.

$$Nu_{lam} = (3.66^3 + 0.7^3 + (1.615(Re_b Pr_b \frac{d_i}{L})^{1/3})^3)^{1/3} \tag{1.5}$$

He showed calculation method for turbulent flow.

$$Nu_{turb} = \frac{\frac{C_{f,turb}}{2Re \cdot Pr_b}}{1 + 12.7\sqrt{\frac{C_{f,turb}}{2}}(Pr_b^{2/3} - 1)} \cdot (\frac{Pr_b}{Pr_w})^{0.11} \tag{1.6}$$

The range is

$$0.1 << Pr_b << 1000, 10^4 << Re_b << 10^6 \tag{1.7}$$

He presented transitional flow as a liner interpolation between turbulent and laminar flow.

$$Nu_m = (1 - r)Nu_{m,lam} + rNu_{m,turb} \tag{1.8}$$

$$r = \frac{Re_b - 2300}{10^4 - 2300} \tag{1.9}$$

第2章　Methodology

2.1 Material properties

2.1.1 Parameters

A 50/50vol% mixture of water and glycole which is a typical liquid coolant in automotive applications were used as a operating fluid. The material properties of the operationg fluid is temperature dependecy. As bigger temperature difference between a pipe wall and the bulk, the material properties pronounced.

specific heat capacity

$$c_p = A_{c_p} + B_{c_p} T = 2.0148 + 4.50E - 3T \tag{2.1}$$

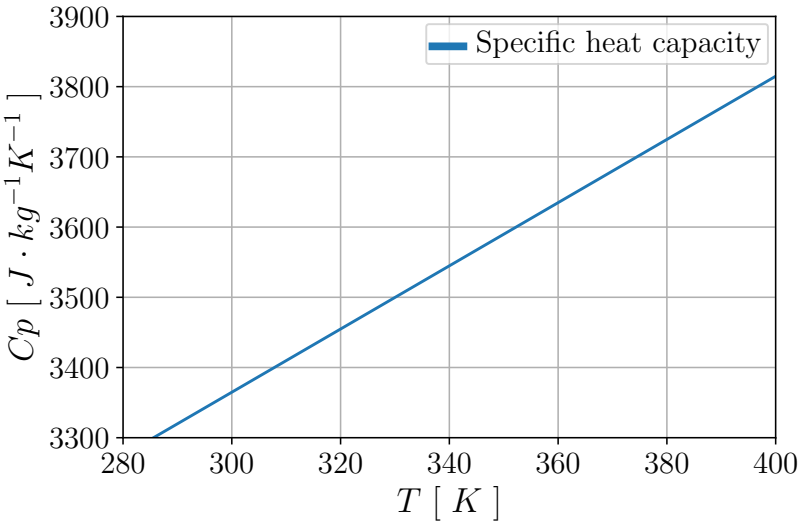

図 2.1: Specific heat capacisty vary with temperature

thermal condictivity

$$\lambda = A_\lambda + B_\lambda T = 0.2134 + 6.071E - 4T \tag{2.2}$$

dynamic viscosity

$$\mu = A_\mu \cdot \exp\left(\frac{B_\mu}{T + C_\mu}\right) = 1.1001E - 4 \exp\left(\frac{325.85}{T - 207.30}\right) \tag{2.3}$$

density

$$\rho = A_\rho + B_\rho T = 1268.28 - 0.66T \tag{2.4}$$

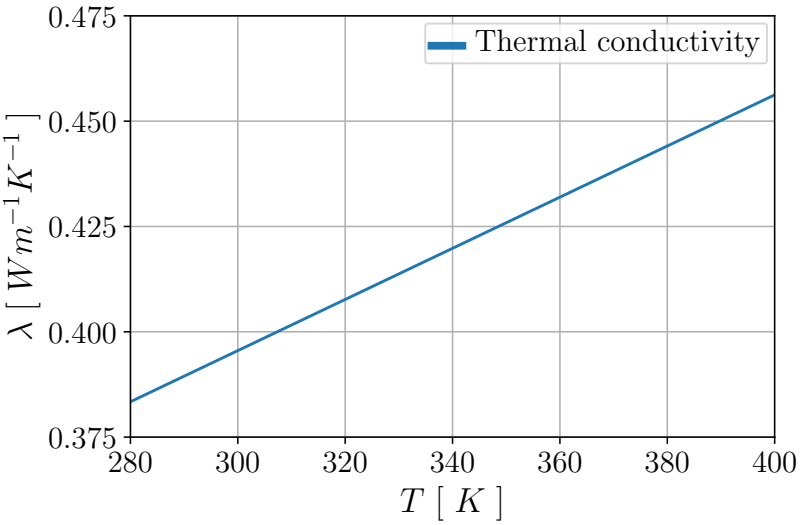

図 2.2: Thermal conductivity vary with temperature

prandtl number

$$Pr = \frac{\nu}{\alpha} = \frac{\mu \cdot c_p}{\lambda} \tag{2.5}$$

2.1.2 Effect of viscosity and density

DNS Effect of viscosity 20% Effect og density 0.5% experimental

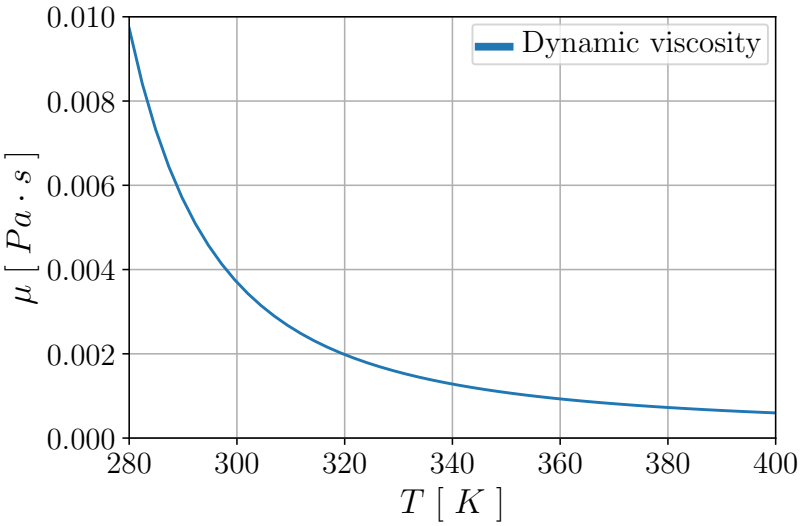

図 2.3: Dynamic viscosity vary with temperature

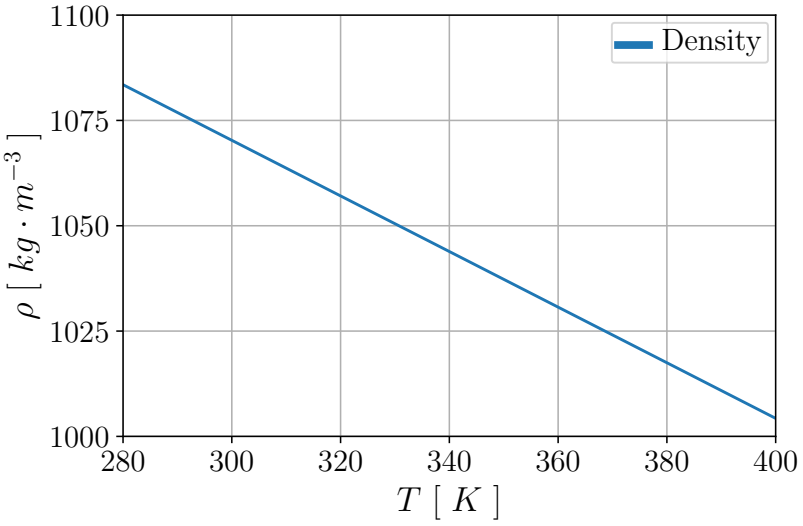

図 2.4: Density vary with temperature

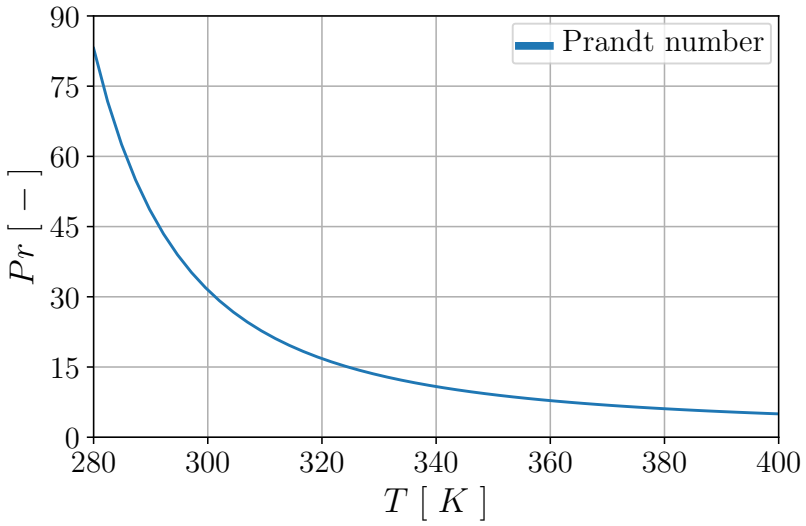

図 2.5: Prandtl number vary with temperature

2.1.3 Cooling and heating

Bertsche et al.[1] shows experimental investigation on heat transfer in cylindrical pipe flow by using a 50/50vol% mixture of water and glycole with cooling. The operationg fluid is the same as our study, however they measured the heat transfer by cooling the liquid. For cooling the liquid, the temperature at the wall is lower than bulk temperature. In other way, for heating the liquid, the temperature at the wall is higher that bulk temperature. As shown in material properties, the viscosity show strong temperature dependence and the curve isn't linear function. Thus, the heat transfer doesn't shows the same value with cooling and heating even though a Prandtl number is the same.

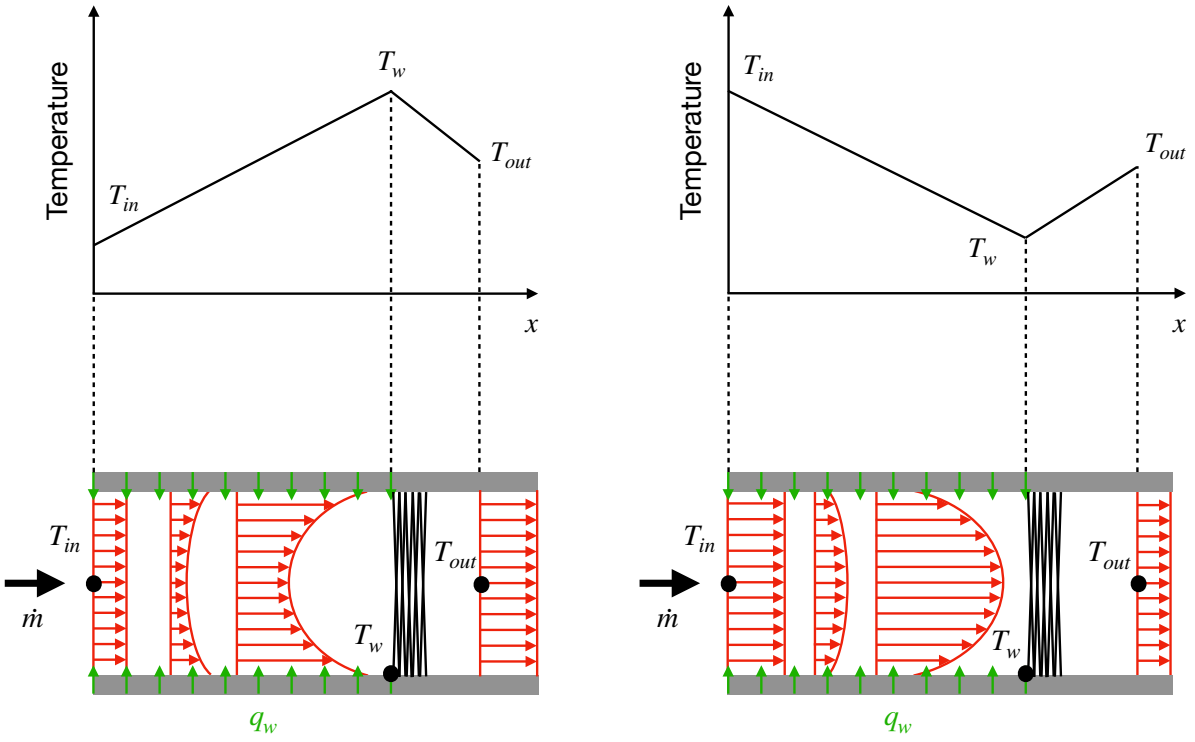

図 2.6: Thermal boundary layer grows in horizontal axis for heating liquid(left) and cooling liquid(right).

2.2 Hydro and thermal boundary layer

第3章　Experimental facilities

3.1 Experimental loop

Figure. 3.1 shows a diagram of the experimental loop. The experimental basically loop consists of a heat exchanger, a pump, a Coriolis mass flow rate, a welder, a reservoir, and a test section. The heat exchanger keeps a thermal stationary condition in the flow pipe. The Coriolis mass flow rate is controlled by the pump and a bypass valve C, which is located in parallel to the pump. The pipe is thermally insulated by using glass wool.

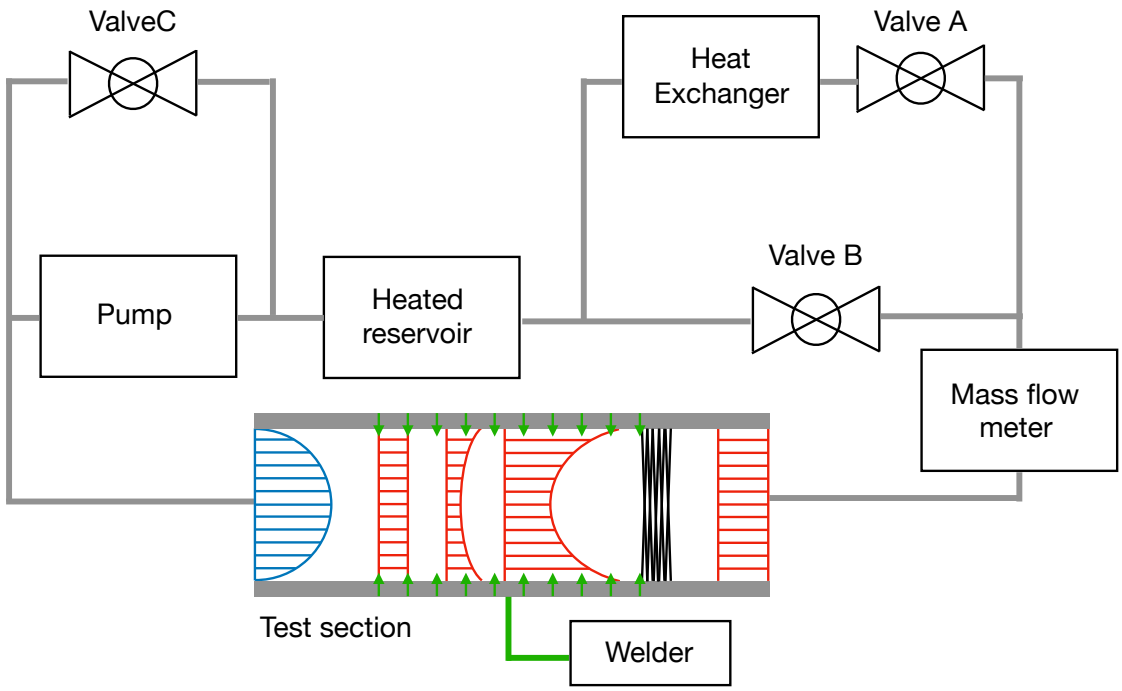

図 3.1: Process flow diagram of the test facilities including test section.

3.2 Test section

3.2.1 Thermal and velocity boundary layer

Figure. 3.2 shows the velocity and thermal boundary layer of developments vary with the horizontal axis in the test section. The velocity and thermal profiles are shown in blue and red

color, respectively. The test section is made of stainless steel (1.4301) with an inner diameter $d_i = 12[mm]$ and outer diameter $d_o = 15[mm]$. Highly accurate resistance thermall probes (PT-100) are used to find out the inlet and outlet bulk temperatures (T_{in}, $T_{out}$and wall temperature (T_w). Moreover, thermocouples (Type-K) are used to measure temperature gradients in the flow direction.

The test section consists of entrance, heated and thermal equalized parts.

1. Entrance part

   The first part of the test section is a 1.2 $[m]$ length entrance part, which is sufficiently long to ensure producing dynamically developed flow condition at the exist. The bulk temperature T_{in} at this section was measured by PT-100.

2. Heated part

   The second part of the test section is a 2.0 $[m]$ length heated part, which is sufficiently long to ensure producing thermal fully developed flow condition at the exist. The tube wall were heated electrically by the welder which provides high current and low voltages to keep the uniform heat flux condition in a inner pipe flow. Convective heat transfer is independent of the horizontal axis in fully developed flow and constant heat flux condition. The wall temperature (T_w) at the end of this section were measured by PT-100.

3. Thermal equalized part

   The third part of the test section is the thermall equalized part, which includes a Static mixture. The static mixture forms turbulent and vortex. Then, the thermal gradients of fluids become averaged, and bull temperature T_{out} is measured.

3.2.2 Length-to-diameter ratio

The length-to-diameter ratio is an important parameter to achieve the fully developed turbulent condition in the test section. The entrance section has an inner diameter of $d_i = 12mm$, and the length of $L = 1.2m$ which length-to-diameter ratio is $L/d_i = 100$. Patel et.al.[8] showed suitable the length-to-diameter ratio for fully developed turbulent flows. According to their study, they found that the minimum developing length of $L/d_i = 70d_i$. Therefore, the length-to-diameter ratio of the entrance section in this experimental is long enough to ensure the fully developed turbulent flow state.

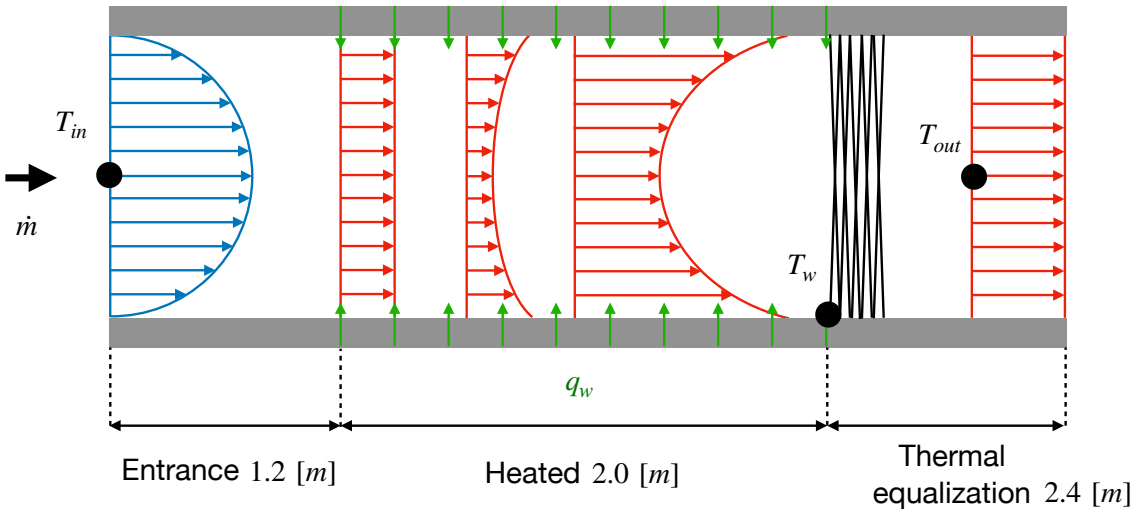

図 3.2: test section

3.3 Conductive heat transfer equation at the pipe wall

3.4 Evaluation procedure

3.5 Uncertainty Analysis of Measurement

Uncertainty of measurement comprises many components such as bias or systematic error and random error in measuring dimension. The measured value for dimension is the sum of true value, bias or systematic error and random error as shown in equation 3.1.

$$x = x_{true} + x_{bias} + x_{random} \tag{3.1}$$

The bias or systematic error may be evaluated from statical distribution and can be characterized by experimental standard deviation. The uncertainty of measurement was discussed by using "Guide to the Expression of Uncertainty in Measurement" [5].

As shown in Chapter ?? in section ??, Reynolds number Re, skin friction coefficient C_f and Nusselt number Nu was calcurated from following equations (3.2)(4.1)(3.6).

$$Re = \frac{UL}{\nu} = \frac{4\rho\dot{m}}{\mu\pi d_i} \tag{3.2}$$

$$C_f = \frac{\tau_w}{\rho_b \frac{U_b^2}{2}},\ \tau_w = \frac{\Delta P}{\Delta z}\frac{d_i}{4},\ U_b = \frac{4\dot{m}}{\rho_b \pi d_i^2} \tag{3.3}$$

$$C_f = \frac{\Delta p}{\Delta z}\frac{d_i^5 \pi^2 \rho_b}{32\dot{m}^2} \tag{3.4}$$

$$Nu = \frac{\alpha d_i}{\lambda} = \frac{q_w d_i}{\lambda\left(T_w - T_{out}\right)},\ q_w = \frac{\dot{m}C_p\left(T_{out} - T_{in}\right)}{d_i \pi L_{heated}} \tag{3.5}$$

$$Nu = \frac{\dot{m}C_{p,b}\left(T_{out} - T_{in}\right)}{\lambda_b\left(T_w - T_{out}\right)\pi L_{heated}} \tag{3.6}$$

Each parameters effect measurement uncertainty in each sensitivity in sensors. The right choice of measurement sensors enable us to reduce measurement uncertainty. However, there is a limitation in reality. Cramer-Rao lower bound (CRLB) theory indicates the smallest uncertainty limit of estimating variance of deterministic process. The maximum possible error in equations (3.2)(4.1)(3.6) can be estimated from measurement data. The uncertainty of skin friction coefficient, C_f is calcurated by equation (3.10).

$$\Delta C_f = \sqrt{\sum\left(\frac{\partial C_f}{\partial X_i}\Delta X_i\right)^2} \tag{3.7}$$

The uncertainty of skin friction coefficient, Nu is calcurated by equation (3.8).

$$\Delta Nu = \sqrt{\sum\left(\frac{\partial Nu}{\partial X_i}\Delta X_i\right)^2} \tag{3.8}$$

Here, $\frac{\partial C_f}{\partial X_i}$ and $\frac{\partial Nu}{\partial X_i}$ represents uncertainty elements and assumed to be statistically independent. In addition, ΔX_i represents absolute error of each sensors. The resulting total measurement uncertaity in skin friction coefficient is shown in equation (3.10)

$$\Delta C_f = \sqrt{\left(\frac{\partial C_f}{\partial \Delta p}\Delta\left(\Delta p\right)\right)^2 + \left(\frac{\partial C_f}{\partial \rho_{out}}\Delta\rho_{out}\right)^2 + \left(\frac{\partial C_f}{\partial \dot{m}}\Delta\dot{m}\right)^2} \tag{3.9}$$

$$= C_f \cdot \sqrt{\left(\frac{\Delta\left(\Delta p\right)}{\Delta p}\right)^2 + \left(\frac{\Delta\rho_{out}}{\rho_{out}}\right)^2 + \left(2\frac{\Delta\dot{m}}{\dot{m}}\right)^2} \tag{3.10}$$

The resulting total measurement uncertaity in Nusselt number is shown in equation (3.8)

$$\Delta Nu = \sqrt{\begin{array}{l}\left(\frac{\partial Nu}{\partial \dot{m}}\Delta\dot{m}\right)^2 + \left(\frac{\partial Nu}{\partial c_{p,out}}\Delta c_{p,out}\right)^2 + \left(\frac{\partial Nu}{\partial \lambda_{out}}\Delta\lambda_{out}\right)^2 + \\ \left(\frac{\partial Nu}{\partial T_{in}}\Delta T_{in}\right)^2 + \left(\frac{\partial Nu}{\partial T_{out}}\Delta T_{out}\right)^2 + \left(\frac{\partial Nu}{\partial T_w}\Delta T_w\right)^2\end{array}} \tag{3.11}$$

$$= Nu \cdot \sqrt{\begin{array}{l}\left(\frac{\Delta\dot{m}}{\dot{m}}\right)^2 + \left(\frac{\Delta c_{p,out}}{c_{p,out}}\right)^2 + \left(\frac{\Delta\lambda_{out}}{\lambda_{out}}\right)^2 + \\ \left(\frac{\Delta T}{T_{in}-T_{out}}\right)^2 + \left(\frac{\Delta T}{T_{out}-T_w}\right)^2 + \left(\frac{\Delta T\left(T_{in}-T_w\right)}{\left(T_{in}-T_{out}\right)\left(T_{out}-T_w\right)}\right)^2\end{array}} \tag{3.12}$$

Table (3.1) shows absolute error for each sensors. As shown in material properties, density, heat capasity and heat conductivity are temperature dependence. Therefore, those absolute error influenced by the sensitivity of the temperature sensor, PT100.

表 3.1: Absolute error of contribution factor of the Reynolds number, skin friction coefficient and Nusselt number.

Contribution	Symbol	Absolute error	Unit
Mass flow rate	$\Delta\dot{m}$	$0.20E-3\dot{m}$	$kg \cdot s^{-1}$
Pressure	$\Delta(\Delta p)$	$0.35E-3\Delta p$	Pa
Temperature	ΔT	0.040	K
Density	$\Delta\rho_{out}$	$0.26E-1$	$kg \cdot m^{-3}$
Thermal conductivity	λ_{out}	$2.4E-5$	$W \cdot m^{-1} \cdot K^{-1}$
Heat capasity	$\Delta c_{p,out}$	0.18	$J \cdot kg^{-1} \cdot K^{-1}$

3.5.1 Case study

In this section, the author showed evaluation procedure to calcurate measurement uncertainty for Reynolds number, skin friction coefficient and Nusselt number, respectively. For this case study, Table (3.2) shows one of the measurement data in this study.

表 3.2: Concrete exaples for evaluation procedure of uncertainty analysis. Comprehensive measurement result of the data is shown in Chapter??.

Case	Pr_w	Re	C_f	Nu	$\dot{m}$	Δp	T_w	T_{in}	T_{out}	ρ_{out}	λ_{out}	$c_{p,out}$
A	10.0	3747	0.0103	39	0.044	254	71.2	65.2	67.6	1041	0.42	3.55
B	10.0	18626	0.0068	152	0.212	3816	71.3	69.5	70.1	1042	0.42	3.56

Measurement uncertainty for Reynolds number was shown in equation —

Measurement uncertainty for skin friction coefficient was shown in equation (3.10). By substituting absolute error shown in table (3.1) into the equation (3.10), which yeilds

$$\Delta C_f = C_f \cdot \sqrt{\left(\frac{0.35E-3\Delta p}{\Delta p}\right)^2 + \left(\frac{0.26E-1}{\rho_{out}}\right)^2 + \left(2\ \frac{0.20E-3\dot{m}}{\dot{m}}\right)^2} \tag{3.13}$$

Then, by substituting measurement data shown in table (3.2)into equation (3.10), measurement uncertainty for skin friction ocefficient is calcurated.

$$\Delta C_f = 0.0103 \cdot \sqrt{\left(\frac{0.35E-3\cdot 253.8}{253.8}\right)^2 + \left(\frac{0.26E-1}{1041}\right)^2 + \left(2\ \frac{0.20E-3\cdot 0.044}{0.044}\right)^2} \tag{3.14}$$

$$= 0.0103 \cdot \sqrt{(0.00035)^2 + (0.0004)^2 + (0.000025)^2} \tag{3.15}$$

$$= 5.5E-6 \tag{3.16}$$

Measurement uncertainty for Nusselt number was shown in equation (3.8). By substituting absolute error shown in table (3.1) into the equation (3.8), which yeilds

$$\Delta Nu = Nu \cdot \sqrt{\begin{array}{c}\left(\frac{0.20E-3\dot{m}}{\dot{m}}\right)^2+\left(\frac{0.18}{c_{p,out}}\right)^2+\left(\frac{2.4E-5}{\lambda_{out}}\right)^2+\\ \left(\frac{0.0040}{T_{in}-T_{out}}\right)^2+\left(\frac{0.0040}{T_{out}-T_w}\right)^2+\left(\frac{0.0040\cdot(T_{in}-T_w)}{(T_{in}-T_{out})\,(T_{out}-T_w)}\right)^2\end{array}} \tag{3.17}$$

$$= 38.7 \cdot \sqrt{\begin{array}{c}\left(\frac{0.20E-3\cdot 0.044}{0.044}\right)^2+\left(\frac{0.18}{3.55E+3}\right)^2+\left(\frac{2.4E-5}{0.420}\right)^2+\\ \left(\frac{0.0040}{65.2-67.6}\right)^2+\left(\frac{0.0040}{67.6-71.2}\right)^2+\left(\frac{0.0040\cdot(65.2-71.2)}{(65.2-67.6)\,(67.6-71.2)}\right)^2\end{array}} \tag{3.18}$$

$$= 38.7 \cdot \sqrt{\begin{array}{c}(0.20E-3)^2+(0.51E-4)^2+(0.57E-4)^2+\\ (0.16E-2)^2+(0.10E-2)^2+(0.27E-2)^2\end{array}} \tag{3.19}$$

$$= 0721 \tag{3.20}$$

第4章　Experiments

4.1 Parameter valiation during experiment

4.2 Validation of experimental result for $Pr_w = 10$

4.2.1 Skin friction coefficient for $Pr_w = 10$

In previous studies friction coefficient have been established by many researches. Since the friction coefficient is independet to temperature and exactly known, validity of the experimental data were checked. Figure (4.1) shows skin frictin coefficient C_f and bulk Reynolds number Re_b for $Pr_w = 10$ compared with DNS and emperical correlations for laminar and turbulent as shown in Equations (1.3)(1.4).

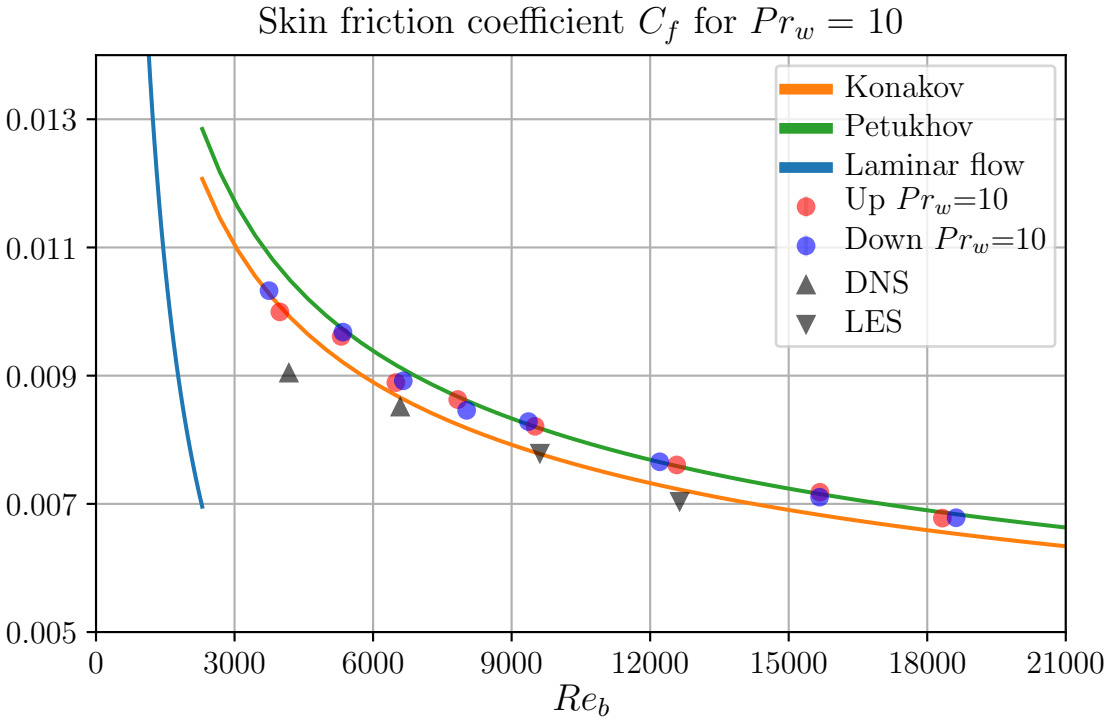

図 4.1: The comparison between skin frictin coefficient C_f and bulk Reynolds number Re_b for $Pr_w = 10$

Every measurement was performed twice to check the reproducibility of the results. The measurement points were taken from lower to higher Reynolds number (red points) and higher to lower Reynolds number (blue points). The reproducibility decreases for lower Reynolds numbers, as can be seen in Figure (4.1).

Each measurement points were averaged value in 420 samples as show in Cahpter??. There was a scattering observed especialy for Low Reynolds number. Detailed discussion is show in Chapter??.

4.2.2 Heat transfer coefficient for $Pr_w = 10$

Figure (4.2) shows heat transfer coefficient Nu and bulk Reynolds number Re_b for $Pr_w = 10$ compared with DNS and Gnielinski correlations for laminar (1.5), transitional (1.8) and turbulent (1.6).

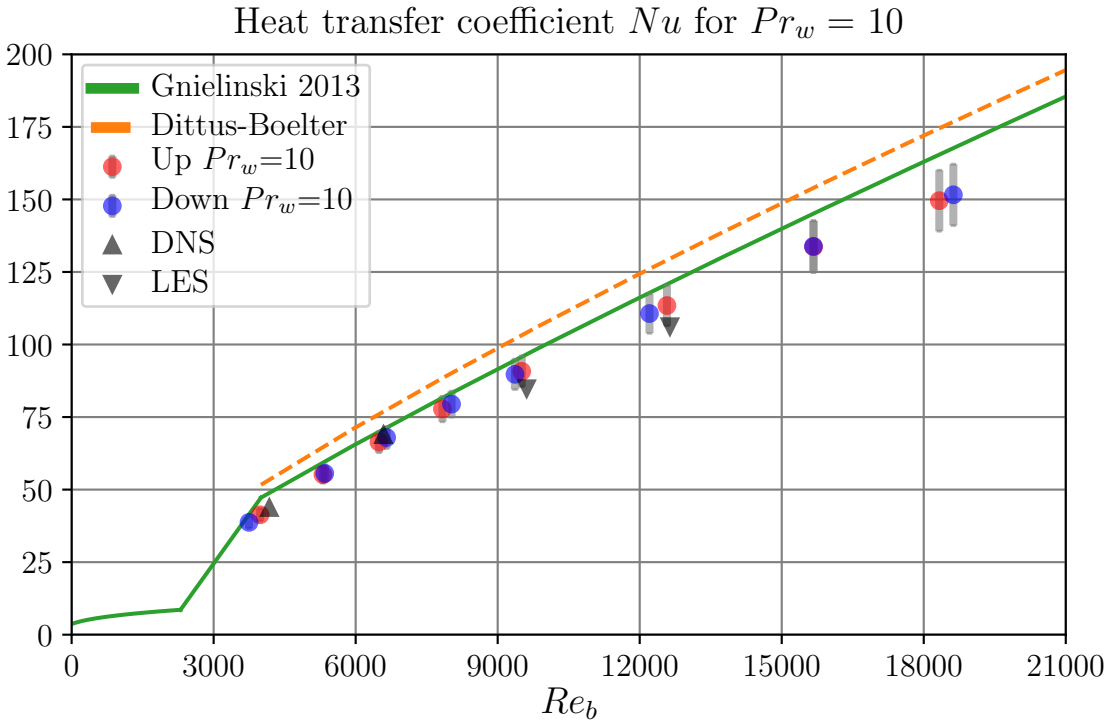

図 4.2: The comparison between heat transfer coefficient Nu and bulk Reynolds number Re_b for $Pr_w = 10$

As mensioned before, every measurement was performed twice to check the reproducibility of the results. A quantitative analysis to determine measurement uncertainties was applied, based on the maximum deviation of the measured and calculated values. Using this approach, the gray error bar in the figures shows measurement uncertainties. The eveluation procedure is shown in Chapter??.

As can be seen in Figure (4.2), it is obvious that the measurement on Nusselt number for $3747 < Re_b < 9508$ are very well fitted by the Gnielinski correlation(1.6). However, for $Re_b > 12207$, the measurement are under estimated and out of the measurement uncertainty.

Table (4.1) shows summary of the experimental parameters for $Pr_w = 10$ and performance of the skin friction coefficient C_f and Nusselt number Nu.

表 4.1: Summary of the experimental parameters for $Pr_w = 10$ and performance of the skin friction coefficient C_f and Nusselt number Nu

Type	Pr_w	Re_b	C_f	Nu	T_{in}	T_{out}	T_w	ΔT	$\Delta\mu/\mu_b$	$q_{w,hc}$
	-	-	$\times 10^{-3}$	-	$^\circ C$	$^\circ C$	$^\circ C$	$^\circ C$	%	kWm^{-2}
Up	10.0	3981	9.99	41.3	65.4	67.8	71.4	3.6	6.2	5.3
	9.9	5309	9.61	55.2	66.4	68.5	71.6	3.1	5.3	6.0
	10.0	6493	8.89	66.4	67.0	68.7	71.3	2.5	4.4	5.9
	10.0	7833	8.63	77.8	67.7	69.1	71.4	2.2	3.9	6.1
	10.0	9508	8.21	90.8	68.1	69.4	71.3	1.9	3.3	6.1
	10.0	12575	7.61	113.4	68.9	69.8	71.4	1.6	2.8	6.4
	10.0	15674	7.18	113.7	69.5	70.2	71.5	1.3	2.2	6.1
	10.0	18328	6.78	149.6	69.6	70.2	71.4	1.2	2.0	6.1
Down	10.0	3747	10.33	38.7	65.2	67.6	71.2	3.6	6.2	4.8
	10.0	5348	9.68	55.6	66.4	68.3	71.2	2.9	4.9	5.6
	10.0	6654	8.92	67.9	67.0	68.7	71.2	2.5	4.3	5.9
	10.0	8026	8.46	79.5	67.7	69.2	71.4	2.2	3.8	6.2
	10.0	9365	8.28	89.7	68.0	69.2	71.2	1.9	3.4	6.1
	10.0	12207	7.66	110.7	68.9	69.9	71.5	1.6	2.8	6.3
	10.0	15668	7.10	113.8	69.3	70.1	71.4	1.3	2.3	6.2
	10.0	18626	6.78	151.6	69.5	70.1	71.3	1.2	2.0	6.2

4.2.3 Skin friction coefficient vary with heat flux for $Pr_w = 10$

Data obtained in previous studies [2] using water as test liquid indicated that providing higher heat flux resulted in lower skin friction coefficient. According to DNS result with using water-glycole, the same trend were observed. In this study, the dependency of wall heat flux were obtained for both skin friction coefficient and heat transfer coefficient. Figure 4.3 shows the results obtained with variety of wall heat flux compared with emperical correlations Petukhov and Konakov [6] and DNS results.

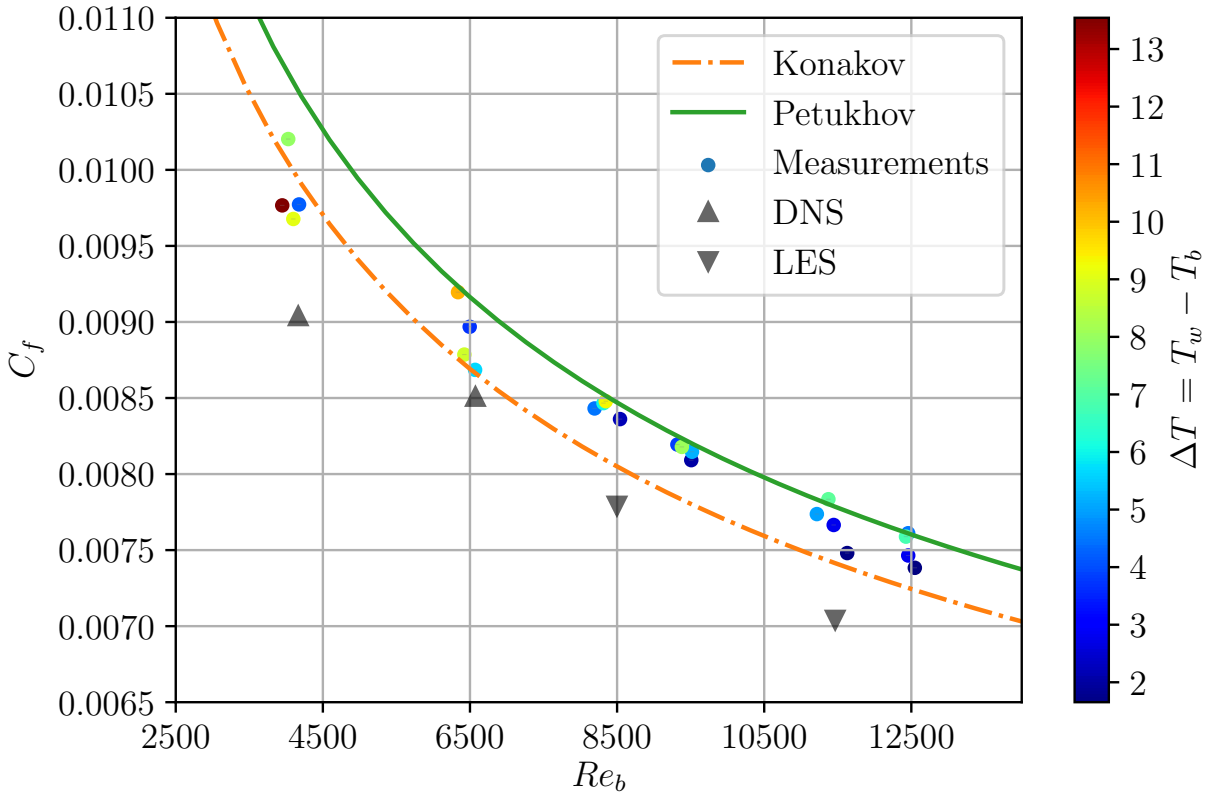

図 4.3: The comparison between skin frictin coefficient C_f and bulk Reynolds number Re_b for $Pr_w = 10$ vary with temperature defference ΔT between a pipe wall T_w and the bulk T_b.

As can be seen,

4.2.4 Heat transfer coefficient vary with heat flux for $Pr_w = 10$

In general, it is apparent that heat transfer coefficient dcrease for higher heat flux.

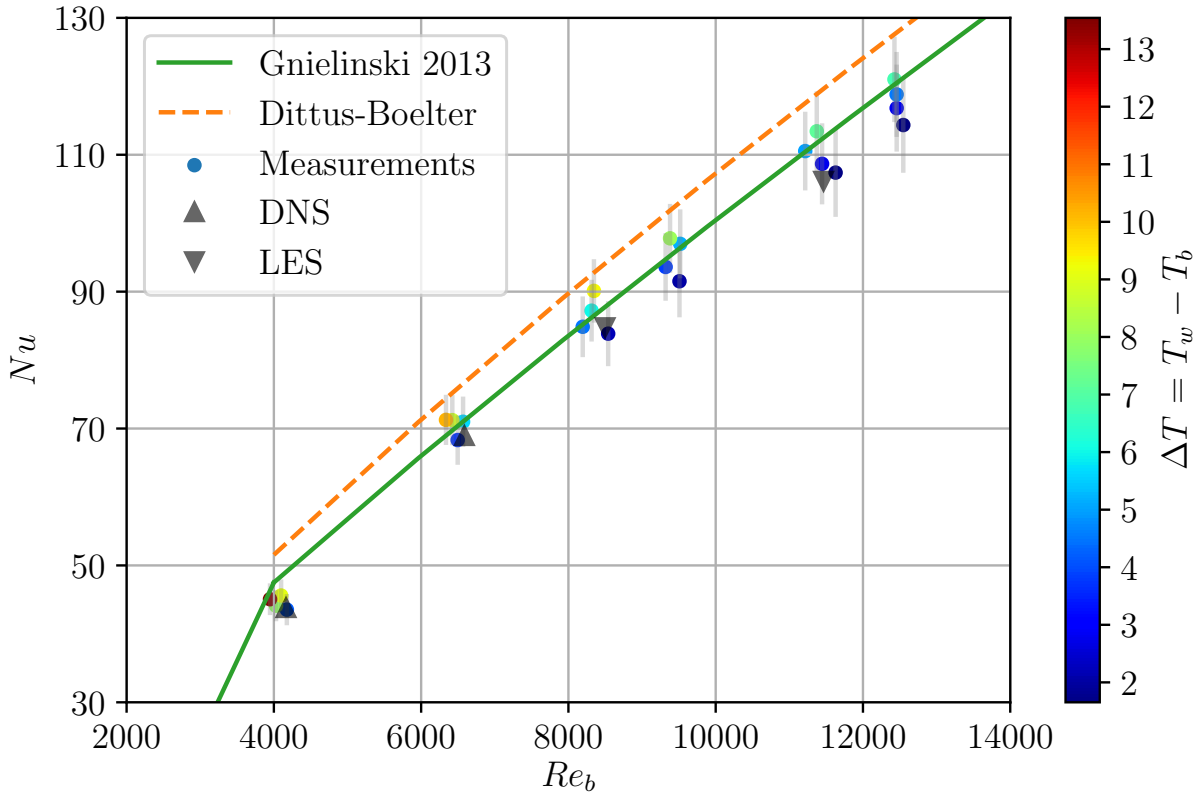

図 4.4: The comparison between heat transfer coefficient Nu and bulk Reynolds number Re_b for $Pr_w = 10$ vary with temperature defference ΔT between a pipe wall T_w and the bulk T_b.

As can be seen,

Table (4.2) summarises the range for Reynolds number and wall heat flux for $Pr_w = 10$ realized during experiments.

表 4.2: Summary of the experimental parameters for $Pr_w = 10$ and performance of the skin friction coefficient C_f, Nusselt number Nu and temperature defference $\Delta T = T_w - T_b$.

Pr_w	Re_b	C_f	Nu	T_{in}	T_{out}	T_w	ΔT	$\Delta\mu/\mu_b$*	q_w**
-	-	$\times 10^{-3}$	-	$^\circ C$	$^\circ C$	$^\circ C$	$^\circ C$	%	kWm^{-2}
10.0	4176	9.77	43.5	64.4	67.2	71.4	4.2	7	6.5
9.9	4029	10.20	44.1	58.9	63.7	71.6	7.9	14	12.3
10.0	4098	9.68	45.6	56.5	62.2	71.3	9.1	16	14.6
10.0	3948	9.77	45.1	49.9	57.9	71.5	13.5	23	21.5
10.0	6496	8.97	68.3	65.3	67.8	71.5	3.7	6	8.9
10.0	6569	8.69	71.0	61.9	65.6	71.3	5.7	10	14.1
9.9	6423	8.79	71.2	57.2	62.8	71.5	8.8	15	22.0
10.0	6337	9.20	71.3	54.8	61.1	71.4	10.2	17	25.6
10.0	8540	8.36	83.9	67.8	69.2	71.5	2.2	4	6.6
10.0	8194	8.43	84.9	64.0	66.9	71.4	4.5	8	13.4
10.0	8315	8.47	87.2	61.6	65.4	71.4	6.0	10	18.5
10.0	8347	8.48	90.1	56.5	62.1	71.4	9.3	16	29.6
9.9	9508	8.09	91.5	68.2	69.5	71.5	2.1	4	6.6
10.0	9320	8.19	93.6	65.1	67.5	71.4	3.9	7	12.8
10.0	9518	8.15	97.0	62.9	66.1	71.3	5.2	9	17.8
9.9	9380	8.18	97.8	58.8	63.6	71.7	8.1	14	27.8
10.0	11628	7.48	107.4	68.8	69.8	71.5	1.7	3	6.5
9.8	11445	7.67	108.7	67.7	69.4	72.1	2.8	5	10.7
10.0	11213	7.74	110.5	63.4	66.4	71.5	5.0	9	19.6
9.9	11373	7.84	113.4	60.4	64.5	71.7	7.2	12	28.7
10.0	12548	7.38	114.3	68.7	69.7	71.4	1.7	3	6.7
10.0	12458	7.46	116.8	66.9	68.6	71.4	2.8	5	11.7
9.9	12457	7.61	118.8	64.5	67.1	71.6	4.5	8	19.0
9.9	12427	7.59	121.0	60.8	64.7	71.6	6.8	12	29.1

表 4.3: Direct Numerical Simuration (DNS) and Large Eggy Simuration (LES) for $Pr_w = 10$ vary with heat flux $q_w = 20$ $[kW/m^2]$ and $q_w =?$ $[kW/m^2]$

Type	Pr_w	Re_τ	Re_b	C_f	Nu	T_w $[°C]$	T_b $[°C]$	ΔT $[°C]$	q_w $[kW/m^2]$
DNS	10.0	360	4165	0.00904	43.8	71.2	58.5	13.1	20.0
DNS	10.0	360	4165	?	?	71.2	?	?	40.0
DNS	10.0	500	6587	0.00851	69.0	71.2	63.3	8.3	20.0
DNS	10.0	500	6587	?	?	71.2	?	?	40.0
LES	10.0	600	8498	0.00779	84.8	71.2	64.8	6.8	20.0
LES	10.0	750	11465	0.00704	106.1	71.2	66.2	5.4	20.0

4.3 Validation of experimental result for $Pr_w = 7, 13$

4.3.1 Skin friction coefficient for $Pr_w = 7, 13$

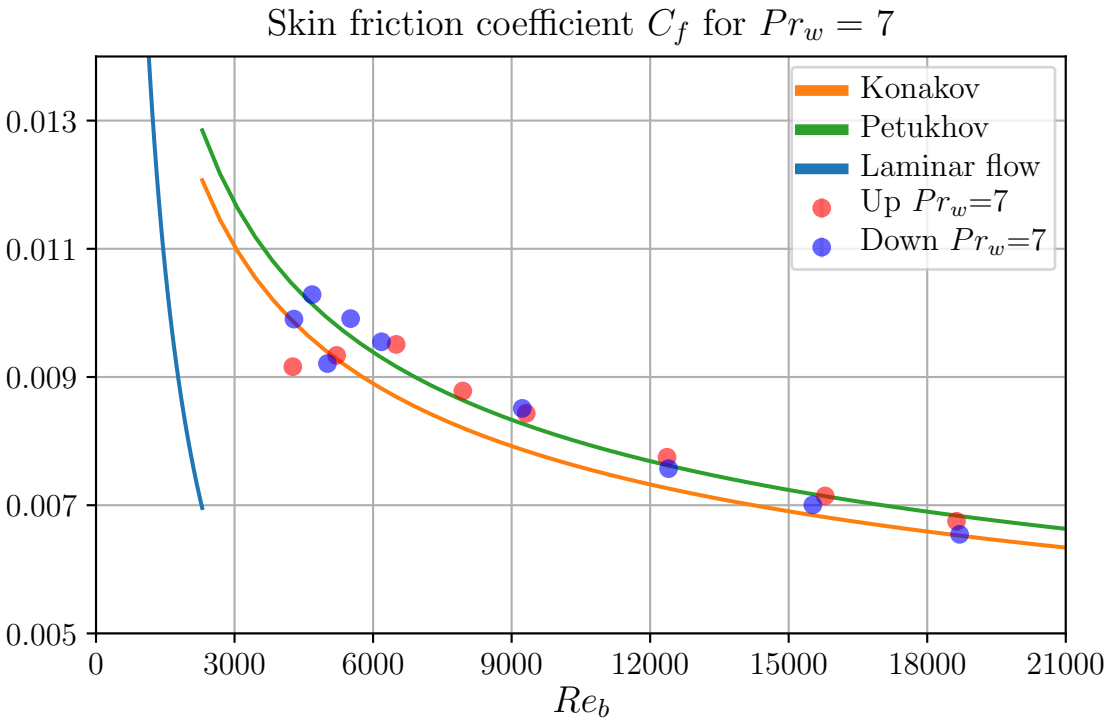

図 4.5: The comparison between skin frictin coefficient C_f and bulk Reynolds number Re_b for $Pr_w = 7$

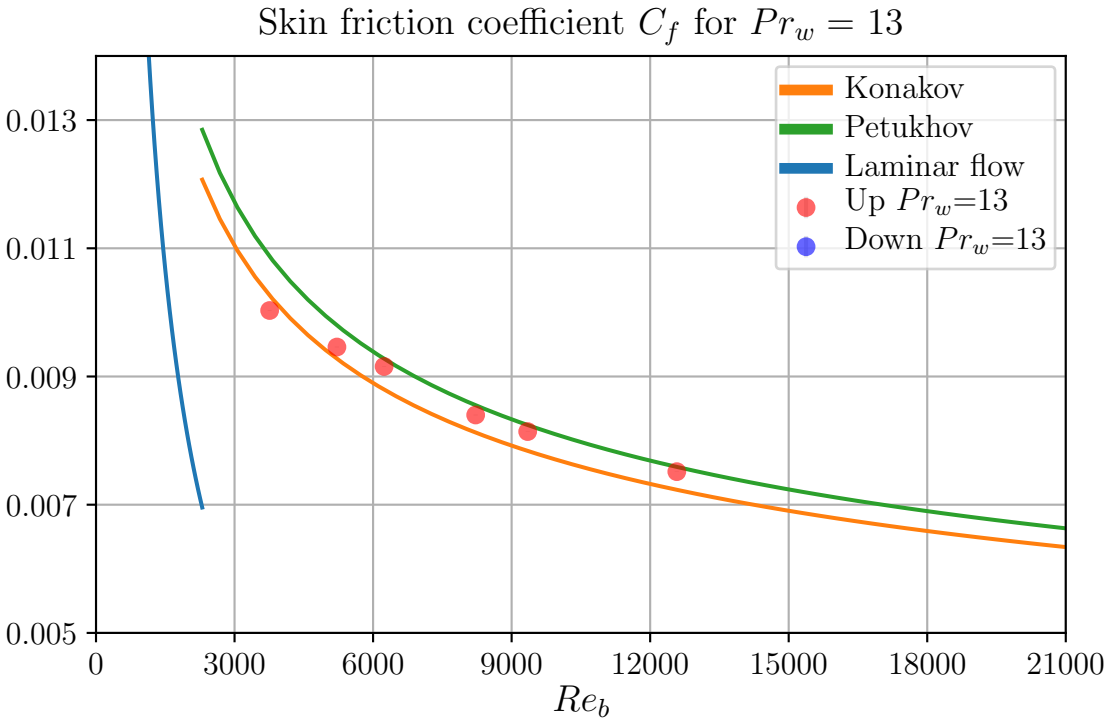

図 4.6: The comparison between skin frictin coefficient C_f and bulk Reynolds number Re_b for $Pr_w = 13$

4.3.2 Heat transfer coefficient for $Pr_w = 7, 13$

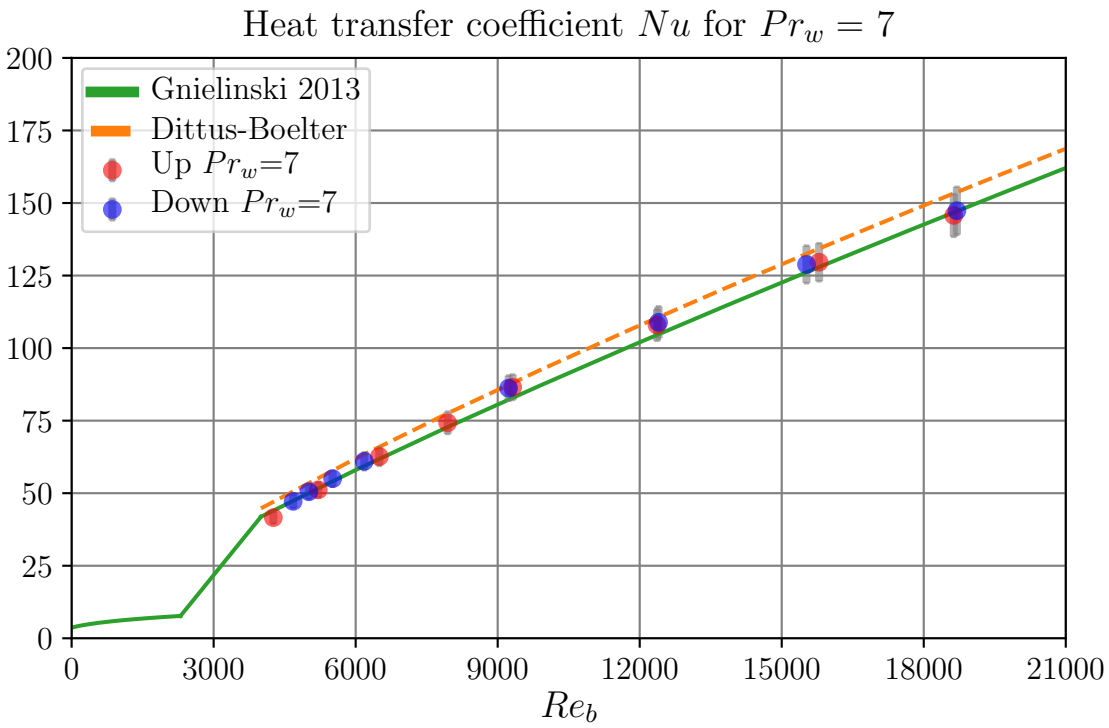

図 4.7: The comparison between heat transfer coefficient Nu and bulk Reynolds number Re_b for $Pr_w = 7$

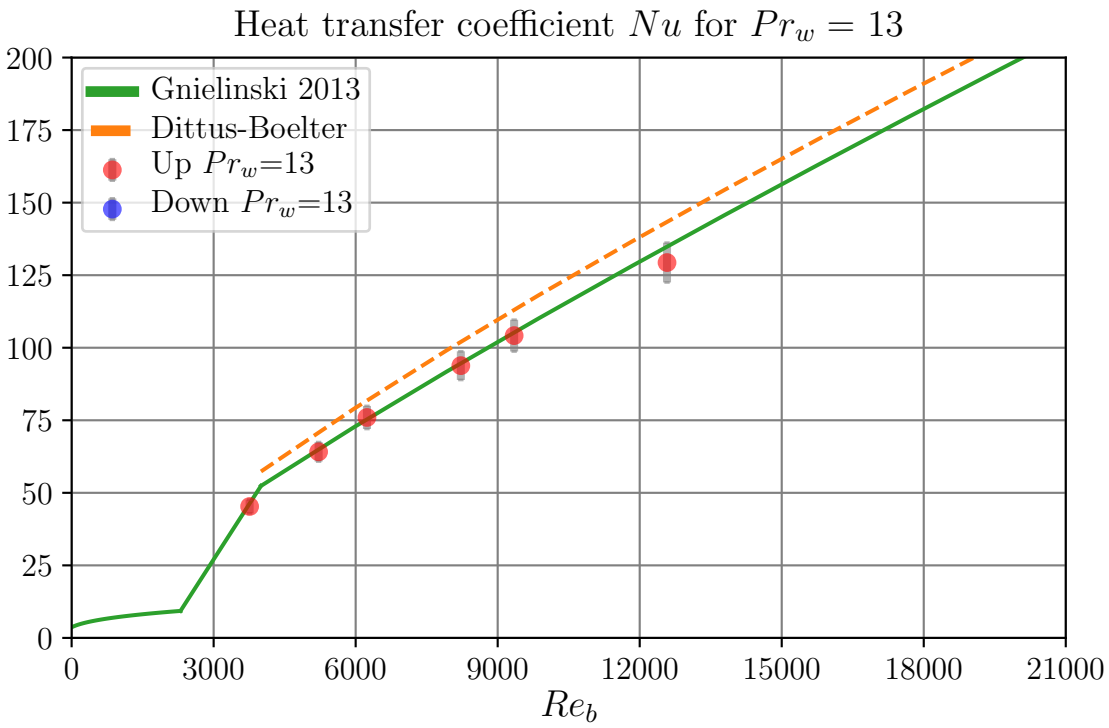

図 4.8: The comparison between heat transfer coefficient Nu and bulk Reynolds number Re_b for $Pr_w = 13$

表 4.4: Summary of the experimental parameters for $Pr_w = 7$ and performance of the skin friction coefficient C_f and Nusselt number Nu

Type	Pr_w	Re_b	C_f	Nu	T_{in}	T_{out}	T_w	ΔT	$\Delta\mu/\mu_b$*	q_w**
	-	-	$\times 10^{-3}$	-	$^\circ C$	$^\circ C$	$^\circ C$	$^\circ C$	%	kWm^{-2}
Up	6.9	4261	9.16	41.6	82.7	88.8	95.7	6.9	8.6	10.0
	7.0	5211	9.34	51.2	84.9	89.8	95.3	5.4	6.8	10.1
	7.0	6500	9.51	62.6	86.8	90.8	95.3	4.5	5.6	10.3
	7.0	7943	8.78	74.3	88.5	91.7	95.4	3.7	4.6	10.0
	7.0	9317	8.43	86.5	84.4	89.3	95.2	5.9	7.4	18.6
	7.0	12366	7.75	108.0	85.3	89.9	95.6	5.6	7.1	22.2
	7.0	15790	7.14	129.6	86.2	90.1	95.4	5.3	6.6	25.1
	7.0	18634	6.75	145.7	86.6	90.2	95.4	5.2	6.5	27.6
Down	7.0	4287	9.90	42.9	77.0	85.5	95.5	10.0	12.5	15.6
	7.0	4385	10.19	44.1	77.2	85.5	95.1	9.6	12.1	15.5
	7.0	4679	10.29	47.2	78.1	86.0	95.1	9.1	11.4	15.6
	7.0	5012	9.21	50.5	78.8	86.3	95.0	8.7	11.0	16.0
	6.9	5513	9.91	55.0	79.3	86.9	95.7	8.8	11.0	17.6
	6.9	6183	9.55	61.0	80.6	87.6	95.7	8.1	10.1	18.0
	7.0	9231	8.51	86.2	83.2	88.6	95.3	6.6	8.3	20.8
	7.0	12399	7.57	108.9	84.3	89.2	95.5	6.3	7.9	25.0
	6.9	15523	7.00	128.8	85.1	89.6	95.7	6.1	7.6	28.7
	7.0	18700	6.55	147.3	91.6	93.2	95.3	2.1	2.7	11.5

* A viscosity ratio of pipe wall and center.$\Delta\mu = \mu_b - \mu_w$.

** Heat flux calcurated from heat capacity equation which directly connected with temperature diff

表 4.5: Summary of the experimental parameters for $Pr_w = 13$ and performance of the skin friction coefficient C_f and Nusselt number Nu

Type	Pr_w	Re_b	C_f	Nu	T_{in}	T_{out}	T_w	ΔT	$\Delta\mu/\mu_b$*	q_w**
	-	-	$\times 10^{-3}$	-	$°C$	$°C$	$°C$	$°C$	%	kWm^{-2}
Up	13.0	3760	10.03	45.3	46.0	50.0	57.7	7.8	16.2	12.1
	13.0	5217	9.46	64.1	45.7	49.9	57.9	8.0	16.6	17.6
	12.9	6239	9.16	76.0	45.6	49.9	58.1	8.2	17.0	21.5
	12.9	8221	8.40	93.8	49.4	52.3	57.9	5.6	11.8	18.3
	12.9	9348	8.14	104.2	49.3	52.3	58.2	5.9	12.3	21.2
	12.9	12577	7.52	129.4	50.9	53.1	57.9	4.8	10.0	21.4
Down										

4.3.3 Skin friction coefficient vary with heat flux for $Pr_w = 7, 13$

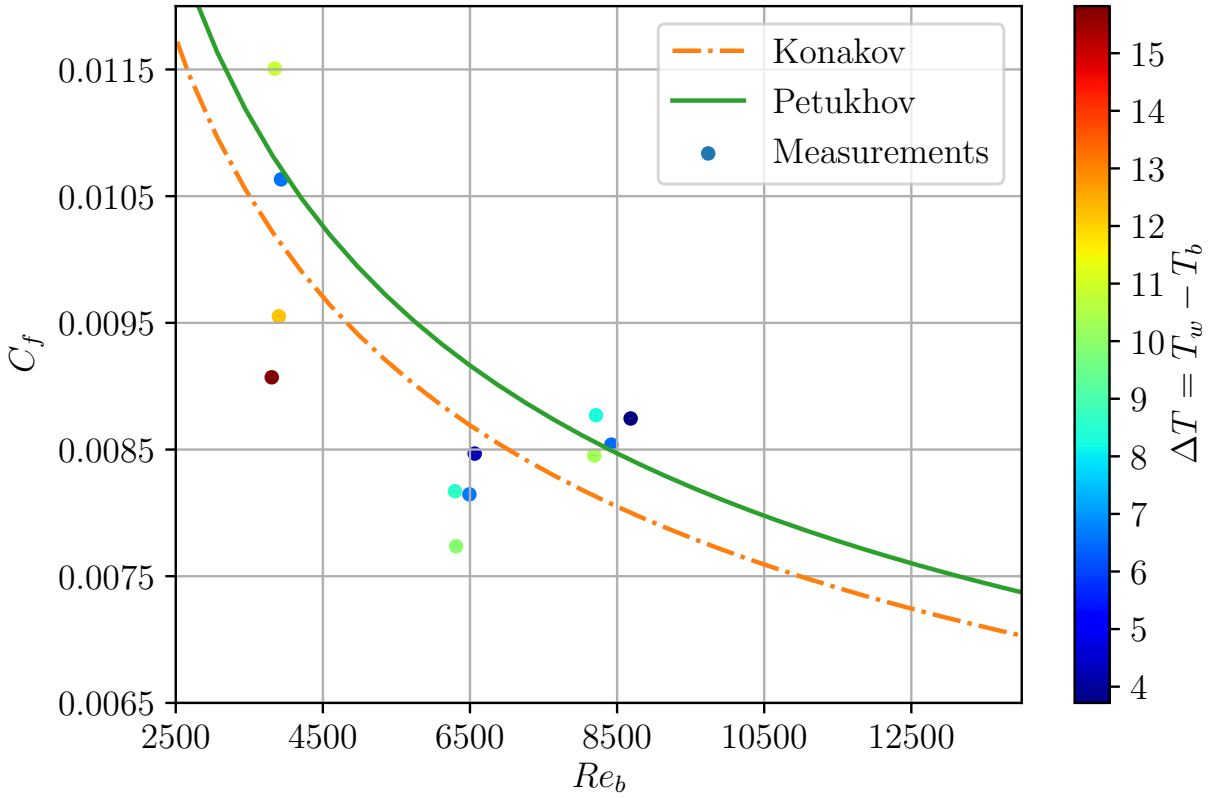

図 4.9: The comparison between skin frictin coefficient C_f and bulk Reynolds number Re_b for $Pr_w = 7$ vary with temperature defference ΔT between a pipe wall T_w and the bulk T_b.

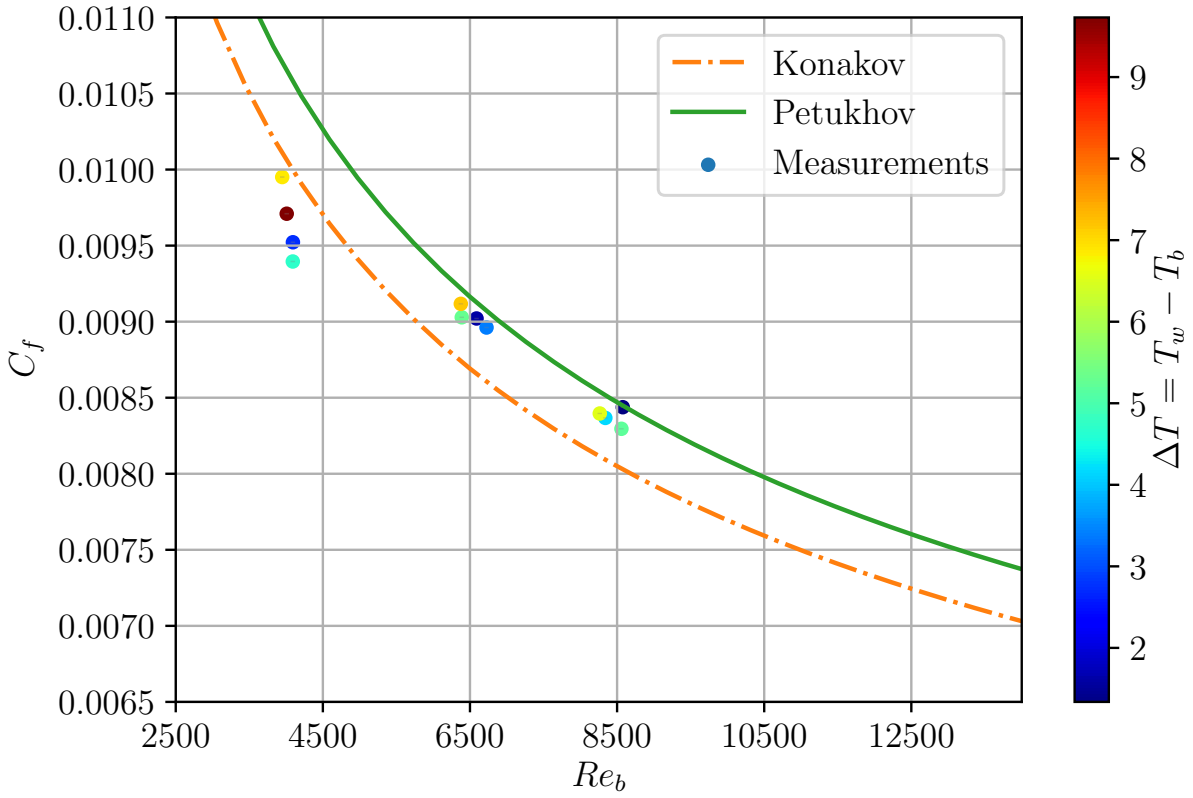

図 4.10: The comparison between skin frictin coefficient C_f and bulk Reynolds number Re_b for $Pr_w = 13$ vary with temperature defference ΔT between a pipe wall T_w and the bulk T_b.

4.3.4 Heat transfer coefficient vary with heat flux for $Pr_w = 7, 13$

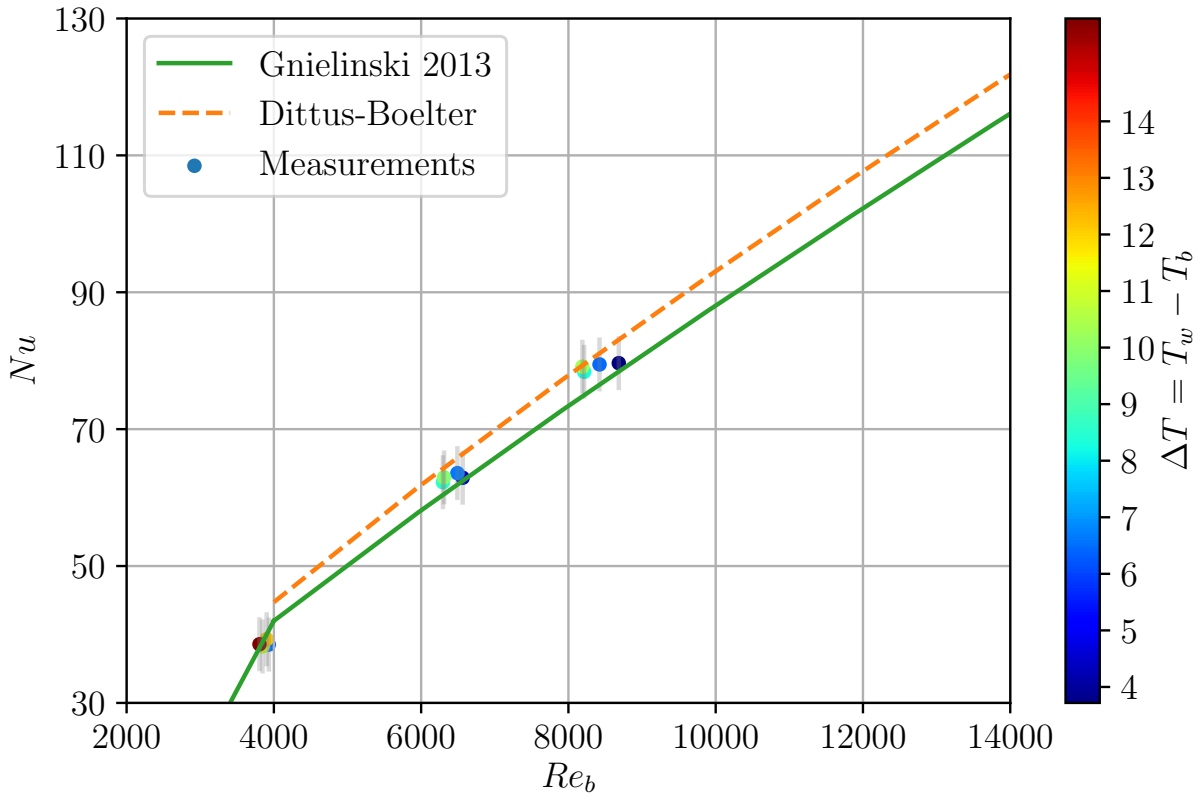

図 4.11: The comparison between heat transfer coefficient Nu and bulk Reynolds number Re_b for $Pr_w = 7$ vary with temperature defference ΔT between a pipe wall T_w and the bulk T_b.

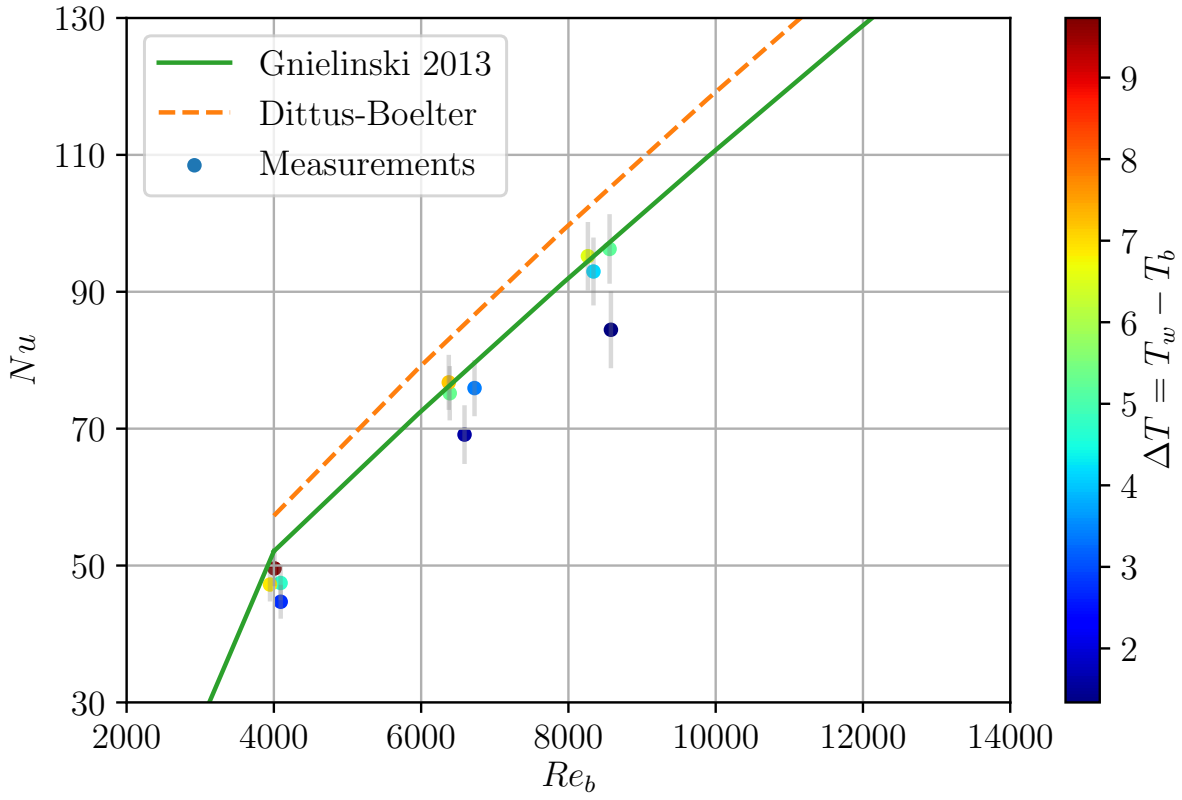

図 4.12: The comparison between heat transfer coefficient Nu and bulk Reynolds number Re_b for $Pr_w = 13$ vary with temperature defference ΔT between a pipe wall T_w and the bulk T_b.

表 4.6: Summary of the experimental parameters for $Pr_w = 7$ and performance of the skin friction coefficient C_f, Nusselt number Nu and temperature defference $\Delta T = T_w - T_b$.

Pr_w	Re_b	C_f	Nu	T_{in}	T_{out}	T_w	ΔT	$\Delta\mu/\mu_b$*	q_w**
-	-	$\times 10^{-3}$	-	$°C$	$°C$	$°C$	$°C$	%	kWm^{-2}
7	4176	9.77	43.5	64.4	67.2	71.4	4.2	7	6.5
7	6496	8.97	68.3	65.3	67.8	71.5	3.7	6	8.9
7	8540	8.36	83.9	67.8	69.2	71.5	2.2	4	6.6
7	9508	8.09	91.5	68.2	69.5	71.5	2.1	4	6.6

表 4.7: Summary of the experimental parameters for $Pr_w = 13$ and performance of the skin friction coefficient C_f, Nusselt number Nu and temperature defference $\Delta T = T_w - T_b$.

Pr_w	Re_b	C_f	Nu	T_{in}	T_{out}	T_w	ΔT	$\Delta\mu/\mu_b$*	q_w**
-	-	$\times 10^{-3}$	-	$^\circ C$	$^\circ C$	$^\circ C$	$^\circ C$	%	kWm^{-2}
13	4176	9.77	43.5	64.4	67.2	71.4	4.2	7	6.5
13	6496	8.97	68.3	65.3	67.8	71.5	3.7	6	8.9
13	8540	8.36	83.9	67.8	69.2	71.5	2.2	4	6.6
13	9508	8.09	91.5	68.2	69.5	71.5	2.1	4	6.6

4.4 Discussion

4.4.1 Reproducibility

4.4.2 Secoundary flow

4.4.3 Electric shield

4.4.4 Trendency of scattering

Figure shows prresure and velocity oscilatin dependence of time axis. Each red crossing points shows measurement samples of each time and the samples were taken every one second.

As shown in figures, both pressure and velocity has fraqutuation dependent of time. In order to investigate the relationship between skin friction coefficient, prresure and velocit, cross correlation function were calcurated. Table show cross correlation for each factors.

Table shows standard deviation of each parameters for Re_b =? ? and Re_b =? ?. As shown in the table, the scattering of those parametes are independ to the Reynolds number. However, the scattering for skin friction coefficient decrease for higher Reynolds number. As shown in Chapter??, skin friction coefficient is deriverded following eqaution. (4.1)

$$C_f = \frac{\Delta p}{\Delta z} \frac{d_i^5 \pi^2 \rho_b}{32 \dot{m}^2} \tag{4.1}$$

The skin fricition coefficiet is proposal to prresure differene Δp and ?? to mass flow rate $\dot{m}$ which is directly connected to valocity$U$. For higher Reynolds number which means higer velosity, skin friction coefficient decrease ??? to the power of mass flow rate. Therefore, the effect of pressure scatering seems to dcrease because of high velocity term.

4.4.5 Electric field from a welder

Skin friction coefficient without heating from the welder could not observe any scattering. The welder achieve high current, and we assumed the scatering come from electric field from the welder. Then, a cable of pressure sensor was surrounded to protect from the eleceric field. Figure shows standard deviation with and without electrical shield. It is ovbsiou that the electical shield achieve to decrease the pressure noise from the welder. Comparing Fig () and (), it is obvious that a significant improvement was obtained in the majority of cases. As you can see from the figures, ???% of the scattering is reduced.

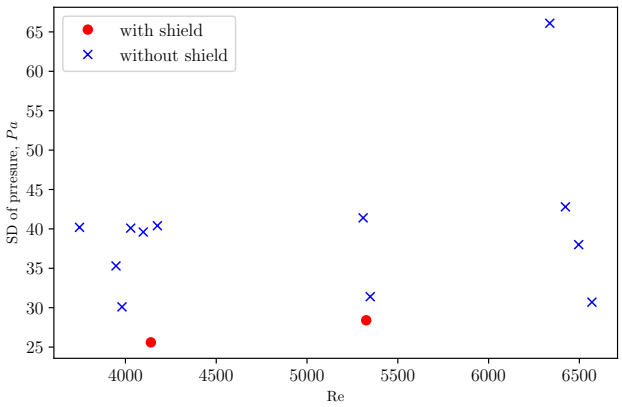

図 4.13: 一つめの図

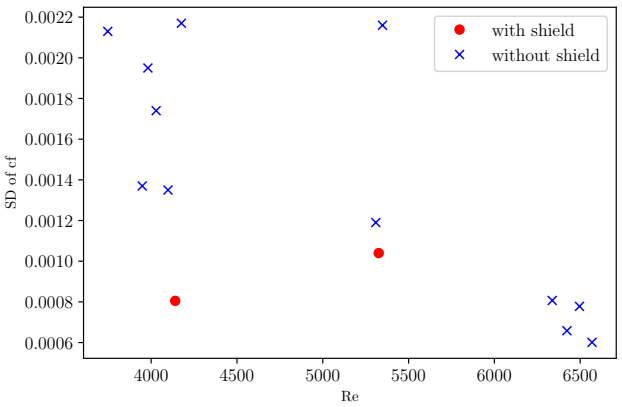

図 4.14: 二つめの図

4.4.6 Probability density function

4.4.7 Comparison with Bertsche

4.4.8 Comparison with DNS and LES

4.4.9 Effect of the presure popower

4.4.10 Effect of material properties

第5章　Conclusion

References

[1] Dirk Bertsche, Paul Knipper, and Thomas Wetzel, *Experimental investigation on heat transfer in laminar, transitional and turbulent circular pipe flow*, International Journal of Heat and Mass Transfer **95** (2016), 1008–1018.

[2] M. Everts and J. P. Meyer, *Relationship between pressure drop and heat transfer of developing and fully developed flow in smooth horizontal circular tubes in the laminar, transitional, quasi-turbulent and turbulent flow regimes*, International Journal of Heat and Mass Transfer **117** (2018), 1231–1250.

[3] V. Gnielinski, *On heat transfer in tubes*, International Journal of Heat and Mass Transfer **63** (2013), 134–140.

[4] Volker Gnielinski, *Neue Gleichungen für den Wärme- und den Stoffübergang in turbulent durchströmten Rohren und Kanälen*, Forschung im Ingenieurwesen **41** (1975), no. 1, 8–16.

[5] JCGM, *Evaluation of measurement data*, International Organization for Standardization Geneva ISBN **50** (2008), no. September, 134.

[6] B. S. Petukhov, *Heat Transfer and Friction in Turbulent Pipe Flow with Variable Physical Properties*, Advances in Heat Transfer **6** (1970), no. C, 503–564.

[7] V. Gnielinski, *New equation for heat and mass transfer in turbulent pipe and channel flow*, International Chemical Engineering **16** (1976), no. 2, 359–368.

[8] E. S. Zanoun, M. Kito, and C. Egbers, *A study on flow transition and development in circular and rectangular ducts*, Journal of Fluids Engineering, Transactions of the ASME **131** (2009), no. 6, 0612041–06120410.